Glaucoma

Vulnerability Zone of Glaucoma Progression in Combined Wide-field Optical Coherence Tomography Event-based Progression Analysis

Won June Lee,[1,2] Ki Ho Park,[3,4] and Mincheol Seong[1,5]

[1]Department of Ophthalmology, Hanyang University College of Medicine, Seoul, Korea
[2]Department of Ophthalmology, Hanyang University Seoul Hospital, Seoul, Korea
[3]Department of Ophthalmology, Seoul National University College of Medicine, Seoul, Korea
[4]Department of Ophthalmology, Seoul National University Hospital, Seoul, Korea
[5]Department of Ophthalmology, Hanyang University Guri Hospital, Guri, Korea

PURPOSE. To investigate the spatial characteristics and patterns of structural progression using the combined retinal nerve fiber layer (RNFL) and ganglion cell–inner plexiform layer event-based progression analysis feature provided by the Guided Progression Analysis (GPA) software of spectral-domain optical coherence tomography.

METHODS. In this retrospective observational study, we evaluated 89 patients with open-angle glaucoma showing clinically confirmed structural progression within a minimum follow-up period of 3 years. For each eye, the RNFL and ganglion cell–inner plexiform layer GPA data were extracted from serial spectral-domain optical coherence tomography (HD-OCT 4000, Carl Zeiss Meditec, Inc., Dublin, CA) data from 2012 to 2017 (available in commercial report). A combined wide-field GPA map was merged using vascular landmark-guided superimposition of RNFL and ganglion cell–inner plexiform layer GPA event-based progression maps onto the RNFL image (resulting in the GPA PanoMaps: proposed in this study). The pattern of progressive structural changes was evaluated by comparing the baseline combined wide-field OCT deviation maps (PanoMap deviation maps: available in commercial report) and GPA PanoMaps at the time the first progression was detected and the GPA PanoMaps at the last follow-up. Spatial characteristics and patterns of glaucoma structural progression on GPA PanoMaps were evaluated.

RESULTS. Progressive structural progression was detected most frequently at the macular vulnerability zone (MVZ), with the peripapillary and macular progression being well-correlated spatially. Compared with the baseline structural change on PanoMap, the progressive structural changes extended toward the fovea at both the peripapillary and macular areas. A spatial difference was observed between the areas where structural damage was frequently found on PanoMap (peripapillary inferoinferior sector and macular MVZ) and areas where progression was frequently found on GPA PanoMap (peripapillary and macular MVZ).

CONCLUSIONS. The patterns of progressive glaucomatous structural changes in both the peripapillary and macular areas were confirmed on the combined wide-field GPA map (GPA PanoMap). An analysis of the progression pattern using the GPA PanoMap facilitates the understanding of the spatial relation between the peripapillary and macular areas in glaucoma.

Keywords: glaucoma, optical coherence tomography, glaucoma progression, PanoMap

To diagnose glaucoma and detect its structural progression, optical coherence tomography (OCT) has been widely used.[1–4] Using the OCT technology and advanced software, ophthalmologists can confirm structural changes in eyes with glaucoma more objectively. Although peripapillary retinal nerve fiber layer (RNFL) has been traditionally used to assess glaucoma damage, recent work has shown significant benefit from the use of macular ganglion cell inner–plexiform layer (GCIPL) analysis.[5–9] More recently, studies have been published on the temporal sequences and spatial relationships between these two areas (peripapillary and macular).[10–14] Some reports introduced that integrating these two areas together using hardware (wide-field scan with swept source technology) or software (scan individually and combine each area together) is useful for diagnosing glaucoma or its progression and can provide more complementary information than using each separately.[11,12,15–19]

Our group reported that a serial analysis of PanoMaps, which integrates the deviation map of the peripapillary and macular areas, performed well in detecting structural

progression in early glaucomatous eyes.[18] Furthermore, our group introduced a combination method, which integrates the peripapillary RNFL and macular GCIPL Guided Progression Analysis (GPA) progression maps, which were derived from glaucoma progression evaluation software (Cirrus HD-OCT GPA software[2,20]), into a single image and helps to evaluate the temporal sequence of the glaucomatous structural progression.[17]

However, no studies using a combined wide-field GPA map (GPA PanoMap) to determine spatial characteristics and patterns of glaucomatous structural progression have been reported to date. The purpose of the present study was to investigate the spatial characteristics and patterns of structural progression using the combined RNFL and GCIPL event-based progression analysis feature provided by the GPA software of spectral-domain OCT.

METHODS

The study protocol was approved by the Institutional Review Board of Seoul National University Hospital (IRB number: H-1904-097-1027). Informed consent was obtained from all patients. The study design followed the tenets of the Declaration of Helsinki for biomedical research.

Patients

For this observational study, we enrolled a total of 89 patients with open-angle glaucoma (OAG) who had shown clinically confirmed structural progression during their respective follow-up periods at the Department of Ophthalmology of Seoul National University Hospital from October 2012 to December 2017. The patients were participants in the Macular Ganglion Cell Imaging Study, which was a prospective study designed in 2011 and is ongoing. From 282 patients in the cohort, 89 patients (31.6%) were enrolled in this study. All the patients underwent a complete ophthalmologic examination, including visual acuity testing, manifest refraction assessment, slit-lamp examination, intraocular pressure measurements using Goldmann applanation tonometry, gonioscopy, dilated fundus examination, axial length measurement (Axis II PR; Quantel Medical, Inc., Bozeman, MT), stereo-disc photography and red-free RNFL photography (TRC-50IX; Topcon Corporation, Tokyo, Japan), Swedish interactive thresholding algorithm 30-2 perimetry (Humphrey Field Analyzer II; Carl Zeiss Meditec, Jena, Germany), and Cirrus HD-OCT (Carl Zeiss Meditec, Inc., Dublin, CA). Both the eyes were imaged with Cirrus HD-OCT and examined with standard automated perimetry every 6 to 12 months for at least 36 months.

Patients with OAG were identified by the presence of a characteristic optic disc (i.e., localized or diffuse neuroretinal rim thinning, increased cupping or cup-to-disc ratio difference of >0.2 between the eyes) on stereo-disc photography, the presence of RNFL defect on red-free fundus imaging regardless of the presence or absence of glaucomatous visual field defects, and an open angle confirmed on gonioscopy.

Progressive optic disc changes (i.e., focal or diffuse rim narrowing, neuroretinal rim notching, increased cup-to-disc ratio, and adjacent vasculature position shift) were determined by comparison of serial stereo-disc photographic images and regarded as indicative of glaucoma progression. Changes in RNFL defects were determined from serial red-free RNFL photographs and defined as the appearance of a new defect or an increase in the width or depth of an existing defect. These changes were regarded as indicative of clinically confirmed structural progression.[21] Two observers (W.J.L., M.S.), who were masked to all other patient information, independently evaluated all the photographs. In cases of a disagreement, a third glaucoma specialist (K.H.P.) served as an adjudicator.

The inclusion criteria were as follows: (1) unilateral or bilateral OAG, (2) clinically confirmed structural progression in the follow-up period, and (3) follow-up examination for more than 36 months with at least four serial RNFL and GCIPL OCT measurements as well as standard automated perimetry. Additionally, patients eligible for inclusion in the study had to have a best-corrected visual acuity of 20/40 or better, spherical equivalent refractive errors from +6.0 to −6.0 diopters, and cylinder correction of less than 3.0 diopters. The exclusion criteria were as follows: a history of ophthalmic surgery (e.g., glaucoma-filtering surgery), any other ocular disease that could interfere with the visual function, any media opacity that would significantly interfere with acquisition of OCT images, inability to obtain a high-quality OCT image (i.e., signal strength of <6), and severe glaucoma showing a mean deviation worse than −20 dB.[22] We excluded severe glaucoma patients for two reasons. First, in the severe stage, there are many diffuse damages on the deviation map. Second, the progression pattern is not well-detected on the GPA owing to the floor effect, especially in the peripapillary RNFL. For cases in which both the eyes met all the eligibility criteria, one eye was randomly chosen as the study eye.

Baseline Structural Damage: Combined Wide-field OCT Deviation Maps (PanoMap Deviation Maps)

The optic disc cube scan (200 × 200 pixels) and ganglion cell analysis protocol for macular cube scanning (6 × 6 mm^2, 200 × 200 pixels) were used for the diagnosis and follow-up of glaucoma. Detailed information on these procedures is available in the literature.[23] With the built-in analysis software (Cirrus HD-OCT software, version 10.0), combined wide-field OCT maps (PanoMaps) could be generated. Baseline structural changes were determined with the combined wide-field OCT deviation maps (PanoMap deviation maps), which automatically integrated the RNFL and GCIPL deviation maps (Fig. 1). Detailed information on these PanoMaps is available in our previously published article.[18]

GPA PanoMap

With the built-in analysis software (Cirrus HD-OCT software, version 10.0), GPA provides event- and trend-based analyses for the detection of progressive thinning of the parapapillary RNFL and macular GCIPL. This method has been described in detail previously.[24] An event-based analysis provides progression maps that represent significant changes (relative to the initial two times baseline data from the third examination) as yellow- or red-colored pixels. In the present study, a combined GPA map was used for single-image evaluation of RNFL and GCIPL progression. The map was created by same-day superimposition of RNFL and GCIPL progression maps onto red-free RNFL photography, as aligned by the Photoshop software (Version 11.0; Adobe, San Jose, CA) based on vascular landmarks, and the
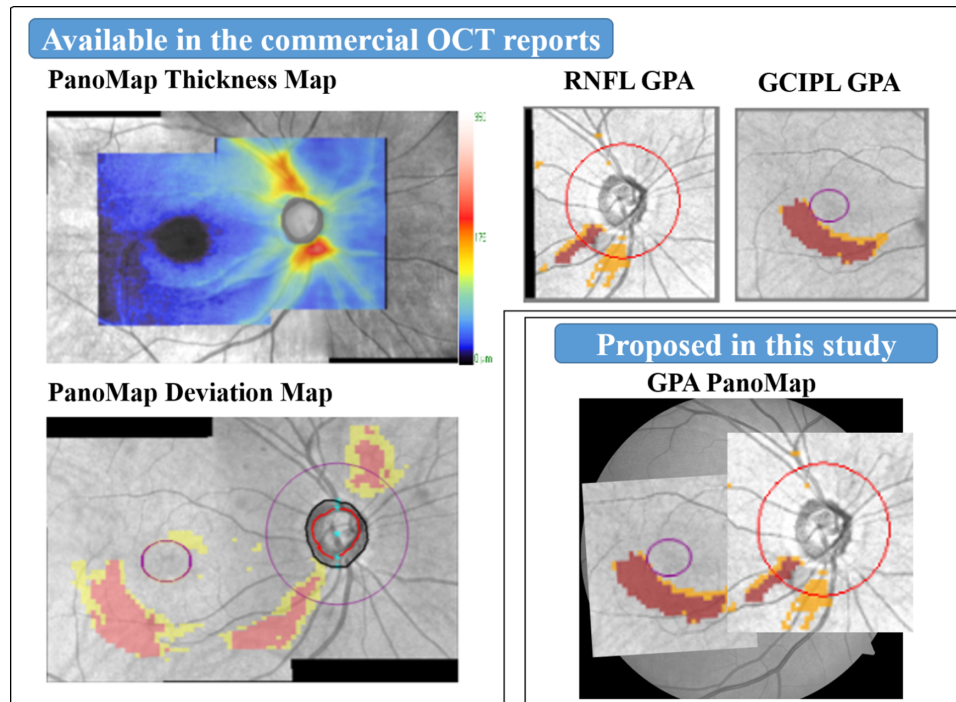
Figure 1. OCT maps used in this study. OCT maps, which are commercially available in Cirrus OCT (PanoMap thickness map, PanoMap deviation map, RNFL-GPA map, GCIPL GPA map and which were proposed in this study (GPA PanoMAP), are shown.

maps were defined as the GPA PanoMap (Fig. 1).[17] Structural progression on the GPA PanoMap was defined as at least 10 contiguous color-coded superpixels on each progression map.[11]

Spatial Characteristics and Patterns of Glaucoma Progression in GPA PanoMaps

To evaluate the overall spatial distribution of progressive structural changes, the color-coded (yellow or red) areas in the GPA PanoMaps of all the enrolled eyes were overlaid after an alignment based on the optic disc and macular center. For aligning the multiple figures with an anatomic variation, a fixed template, which was based on previous studies, was used.[10,17,25] Based on two anatomic landmarks (optic disc and macular center), the original GPA PanoMaps were stretched and tilted to fit the template (This aligning concept was applied with reference to previous research[25]). Subsequently, modeled GPA PanoMaps were merged for statistical analysis. The maps were aligned based on the right eye's orientation (Supplementary Fig. S1).

To evaluate the spatial changes in the progression over time, GPA PanoMaps were merged and analyzed at the time of the first structural change detected on GPA PanoMap and at the time of the last visit. To compare the spatial distribution between baseline structural changes and progressive structural changes on GPA PanoMap, the baseline PanoMap deviation maps were overlaid and analyzed in the same manner To evaluate which sector changes (both baseline structural changes and progressive structural changes) occurred most frequently, we applied a modified template based on previous studies.[10,17,25] Sectors were divided into the superior vulnerability zone (SVZ), peripapillary papil-

lomacular bundle, peripapillary macular vulnerability zone (MVZ), inferoinferior zone, macular peripapillary papillomacular bundle, and macular MVZ (Supplementary Fig. S2).

Statistical Analyses

Statistical tests were performed using IBM SPSS Statistics 24 (IBM Corp, Armonk, NY). For image merging and analyzing the spatial distribution, R imager, rasterImage (R package), and R version 3.61 (The R Foundation for Statistical Computing, Vienna, Austria) were used. Two visualizing methods were used to show the results effectively: (1) the frequency plots were directly drawn to confirm the distribution pattern (Fig. 2) and (2) the schematic figures showing only the portion above the arbitrary set cut-off value were drawn (Fig. 3). To describe the location of frequency distribution plots, the peripapillary RNFL was expressed as an angle from the center of optic disc, and the macular GCIPL was expressed as an angle from the foveal center. The angle was measured counterclockwise from the horizontal meridian. To see the difference in frequent occurring area at each time point, χ^2 tests were used.

RESULTS

The study included 89 eyes with OAG that met the inclusion criteria.

Clinical Demographics

Table 1 shows the clinical demographics of all patients at the time of enrollment. The average number of OCT scans was 5.4 ± 0.9 (range, 4–7), and the average follow-up period
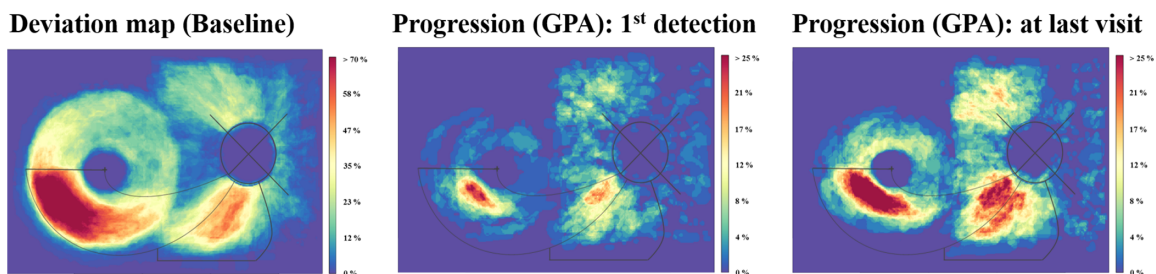
FIGURE 2. Frequency distribution plots of progressive structural changes in combined GPA PanoMap. The overall spatial distribution of the baseline structural damage and progressive structural progression were displayed by overlaying the color-coded areas on the baseline PanoMap deviation map and GPA PanoMaps (at the time of the first structural change detected on GPA PanoMap and at the time of the last visit) as the frequency distribution plots.
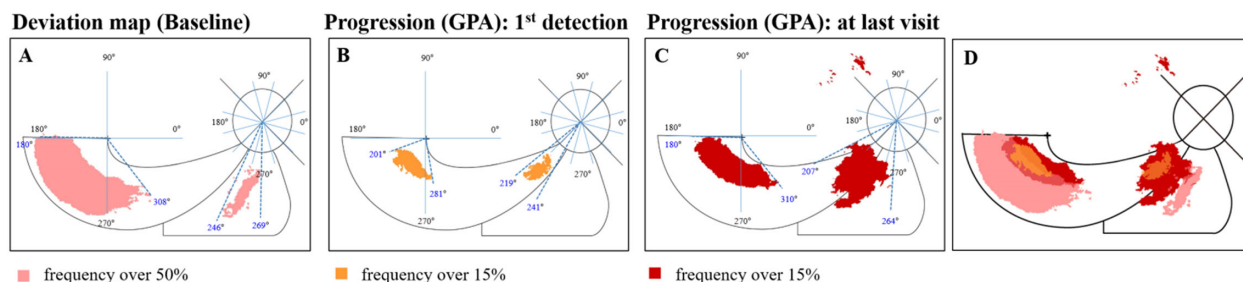
FIGURE 3. Summaries of the spatial distribution of areas where the structural progression frequently occurs. The overall spatial distribution of the baseline structural damage (PanoMap deviation map) is presented (**A**). The inferotemporal peripapillary sector is the most frequent location where progressive RNFL thinning is evident, and the inferotemporal macular area is the most susceptible region for progressive macular GCIPL changes, where the first progression has been detected on the GPA PanoMap (**B**). At the last visit, the most frequent area where the GPA PanoMap shows structural progression is widened compared with initial progression-detected area both in the peripapillary and macular areas (**C**). Progressive structural progression is detected most frequently at the MVZ, with peripapillary and macular progression being well-correlated (connected) spatially (**B** and **C**). To make the direct comparison easier, three images have been superimposed (**D**).

TABLE 1. Clinical Demographic Characteristics of Glaucoma Patients

	Mean ± Standard Deviation (n = 89) or No. (%)	Range
Age (years)	52.1 ± 13.5	22–81
Male sex	46 (51.7)	—
OCT scan number	5.4 ± 0.9	4–7
Follow-up period (mo)	57.9 ± 7.5	36–75
Time difference between initial progression and last follow-up (mo)	20.0 ± 12.7	0–46
Baseline visual field parameters		
Mean deviation (dB)	−2.98 ± 3.58	−15.57–2.95
Pattern standard deviation (dB)	5.09 ± 4.09	1.34–15.94
Visual field index (%)	93.3 ± 8.7	55–100
Baseline RNFL thickness (μm)	80.4 ± 10.2	60–104
Baseline GCIPL thickness (μm)	74.0 ± 6.4	56–92
RNFL GPA		
Average RNFL thinning rate (μm/y)	−1.42 ± 0.90	−4.78–0.33
Superior RNFL thinning rate (μm/y)	−1.88 ± 1.45	−6.42–1.01
Inferior RNFL thinning rate (μm/y)	−2.37 ± 2.07	−10.88–1.38
GCIPL GPA		
Average GCIPL thinning rate (μm/y)	−0.87 ± 0.55	−2.94–0.17
Superior GCIPL thinning rate (μm/y)	−0.72 ± 0.78	−4.73–0.81
Inferior GCIPL thinning rate (μm/y)	−1.03 ± 0.73	−3.66–0.55
Disc hemorrhage during follow-up	41 (46.1%)	
FDA (°)	5.97 ± 3.59	−5.93–16.19

TABLE 2. The Frequency of Structural Changes by Sectors in Combined Wide-field OCT

| | PanoMap Deviation Map | GPA PanoMap | |
	Baseline Structural Damage	At First Detected Progression	At Last Follow-up Progression
SVZ	45 (50.6%)	32 (36.0%)	44 (49.4%)
Peripapillary PM	13 (14.6%)	19 (21.3%)	30 (33.7%)
Peripapillary MVZ	38 (42.7%)	39 (43.8%)	43 (48.3%)
Inferoinferior	73 (82.0%)	24 (27.0%)	30 (33.7%)
Macular PM	40 (44.9%)	12 (13.5%)	25 (28.1%)
Macular MVZ	84 (94.4%)	34 (38.2%)	54 (60.7%)

$P < 0.001$.
For defining the sectors, we applied modified-template which was based on previous studies.[10,17,25] (Supplementary Fig. S2).
PM, papillomacular bundle.

was 57.9 ± 7.5 months (range, 36–75 months). Among the 89 eyes showing clinically confirmed structural progression, 41 (46.1%) presented with disc hemorrhage in the follow-up period. The average fovea-disc angle (FDA) was $5.97 \pm 3.59°$ (range, $-5.93°$ to $16.19°$).

Progressive Structural Changes in the Combined GPA (GPA PanoMap)

The overall spatial distribution of baseline structural damage and progressive structural progression were displayed by overlaying the color-coded areas in the baseline PanoMap deviation map and GPA PanoMaps (at the time of the first structural change detected on GPA PanoMap and at the time of the last visit) as the frequency distribution plots (Fig. 2). In constructing Figure 2, a frequency scale was arbitrarily selected to well-visualized the frequent location in both the peripapillary and macular areas (from 0 to >70% on PanoMap deviation map and from 0 to >25% on GPA PanoMaps). Figure 3A, B, and C schematically summarizes the spatial distribution of areas where structural progression frequently occurred. In constructing Figure 3, the numeric values represented by the colored area was arbitrarily selected to well-visualized the frequent location in both the peripapillary and macular areas (>50% on PanoMap deviation map, >15% on GPA PanoMaps). Additional figures with different cut-off values using the same data were presented in Supplementary Figure S3. For direct comparisons of spatial distributions between the PanoMap deviation map and GPA PanoMaps, each map was superimposed on each other and visualized in Figure 3D.

The results of the frequency of structural changes by sector are shown in Table 2. In the baseline PanoMap deviation map, the frequency was highest in macular MVZ, followed by inferoinferior zone and SVZ (94.4%, 82.0%, and 50.6%, respectively). In the GPA PanoMap at the first progression was detected, the frequency was highest in peripapillary MVZ, followed by macular MVZ and SVZ (43.8%, 38.2%, and 36.0%, respectively). At the last visit, the most frequent progressed sectors were macular MVZ, SVZ, and peripapillary MVZ (60.7%, 49.4%, and 48.3%, respectively). Sectors with most frequent structural changes were different at each of the three time points, and it was statistically significant ($P < 0.001$).

The inferotemporal peripapillary sector at 219° to 241° was the most frequent location where progressive RNFL thinning was evident, and the inferotemporal macular area at 201° to 281° was the most susceptible region for progres-

sive macular GCIPL change, where the first progression was detected on the GPA PanoMap (Fig. 3B). Compared with the overall spatial distribution of the baseline structural damage (PanoMap deviation map), which was detected most frequently in the inferotemporal peripapillary area (246°–269°) from the disc center (RNFL) and in the inferotemporal macular area (180°–308°) from the foveal center (GCIPL) (Fig. 3A), the progressive structural change extended toward the fovea (centripetally) at both, the peripapillary and macular areas (Fig. 3D). At the last visit, the most frequent area where the GPA PanoMap shows structural progression was widened compared with the area where the initial progression was detected, both in the peripapillary and macular areas (Fig. 3C and 3D).

Progressive structural progression was detected most frequently in the MVZ, with the peripapillary and macular progression being well-correlated (connected) spatially (Figs. 3B and 3C).

Discussion

This study was prompted by recent findings indicating that (1) the concept of integrating the peripapillary and macular areas and the concept of some vulnerability zone, such as MVZ, has been emerging[10–13,19]; (2) baseline structural changes in the deviation map and progression on the GPA map could be different in each peripapillary area or macular area[3,20,24,26,27]; and (3) the GPA PanoMap, in which integration of peripapillary RNFL GPA and macular GCIPL GPA, is useful for understanding progression patterns in glaucoma.[17] To further validate the relevant previous results, we attempted to investigate the spatial characteristics and patterns of structural progression using the combined RNFL and GCIPL event-based progression analysis feature provided by the GPA software.

Using the baseline PanoMap deviation map, glaucomatous structural damage was more frequently observed in the macular area than in the peripapillary area. In addition, the peripapillary and macular damaged areas, which were observed on the PanoMap deviation map, were not well-linked spatially. It is possible that the structural changes of peripapillary and macular area may not have occurred simultaneously; rather, it can be an independent change that was coincident in time. Kim et al.[11,12] reported that detection of the inferior macular GCIPL loss might be earlier than that of the peripapillary RNFL defect in MVZ. Similar results have been observed in our study, which may be associated with the fact that most enrolled patients have early glaucoma. We suggested two reasons why the

patterns on peripapillary RNFL and macular GCIPL damage on PanoMap deviation map differ. First, structural damage occurred at different locations. One is on the inferoinferior RNFL pathway; therefore, only the peripapillary RNFL map could detect this damage. At that damage area, GCIPL associated with inferoinferior RNFL are located outside of macular area. Another damaged area is on the MVZ RNFL pathway. At that site, structural damage could be detected earlier in macular GCIPL map.[11,28] At the peripapillary MVZ area, many RNFL fibers are condensed in a very narrow area. However, the GCIPL associated with MVZ spread more sparsely at the macular area. Therefore, early changes of decline in macular GCIPL are detected well in the macular GCIPL map, but those changes are not detected in the peripapillary RNFL map because they are tiny changes in a very condensed and crowded peripapillary MVZ area. Second, the separate peripapillary RNFL deviation map and macular GCIPL deviation map are generated based on their own normative database, which does not consider the continuous linking between peripapillary RNFL and macular GCIPL. Each area's normative database was only based on the horizontality; anatomic variation in the spatial distribution between optic disc and macula was not considered. As a result, the damages occurring in same dendrite–soma–axon complex could not be spatially linked to each other in PanoMap, which is composed of two separate deviations maps with their own normative database.

In contrast, progression of glaucomatous structural damage, which was evaluated on the GPA PanoMap, was frequently observed in the area of MVZ, and the progressed area in peripapillary and macular areas were well-correlated spatially through the anatomic RNFL pathway. The spatial relationship between the peripapillary and macular areas was more evident in the progression than in the initial structural damage. This may mean that the structural damage "progresses" mainly in the MVZ in the patient who has been diagnosed with glaucoma. Depending on the location and severity of the initial structural damage, this progression may be classified into "new onset," "widening," and "deepening."[17,24] Hood et al.[13] recently introduced the concept of the MVZ, which denotes a narrow region of the disc that is associated with the structural damage of the macula, found in early glaucoma. Our study extends the previous concept of the MVZ by showing that the MVZ area, including both the peripapillary and macula areas, is an area of frequent progression.

The deviation map shows the damaged area by statistically comparing the patients' data with the embedded normative database in an area (peripapillary and macular areas separately). Considering the spatial continuity between the optic disc and the macular structure, the use of a uniform normative database that does not consider the individual anatomic variations has limitations. The FDA, determined by the horizontal meridian through the center of the optic nerve head and the axis passing through the fovea and optic nerve head center, varies across patients, and this axis would be associated with the nerve fiber distribution.[29] Similarly, in this study, the axis values were observed variously in both the PanoMap implemented by the embedded software and the GPA PanoMap, which manually combined the GPA of two areas. Although it is difficult to show uniformity because the RNFL distribution varies from patient to patient (including patients with myopia), it is theoretically reasonable to use a normative database modified according to the FDA for considering RNFL pathway rather than the current

uniformed normative database based on horizontality. The distance between the fovea and the optic disc center was also associated with the RNFL profile.[30] The PanoMap was implemented by taking the deviation map from each normative database of two areas without accounting for individual anatomic variations and, subsequently, overlapping the two images based on the vascular structures. Even in cases of the wide-field deviation map (SuperPixel Map) provided by swept-source OCT, the protocol uses a normative database of each separate area (peripapillary and macula areas) rather than the normative database of a wide-field area and, subsequently, combines each image.[15,16] This aspect needs to be overcome through technological development that can consider anatomic variations and collection of the wide-field normative database.

Because the aim of this study was to investigate the structural relationship between the optic disc and the macula in relation to the RNFL pathway, we tried to unify each anatomic variation through the template proposed by Hood et al.[10,17] We also applied the mean FDA in the enrolled eyes (6°) to the template to better visualize the average glaucomatous structural damage and progression.

The spatial relationship between the peripapillary and macular area is more evident on the GPA PanoMap (progression) than on the PanoMap deviation map (initial structural damage), which could be due to the following reasons. On the GPA PanoMap, the map is generated by comparing the data with each own baseline data rather than the normative database, so that a more accurate "real" progression area can be visualized. Individual GPA (RNFL GPA and GCIPL GPA) also does not consider the FDA and it does not need to consider the anatomic variations when combining two GPAs. The progression in same dendrite–soma–axon complex could be detected simultaneously in both peripapillary RNFL and macular GCIPL GPA map and spatial relation between two landmarks is well correlated compared with those in PanoMap.

Previous studies have examined the structural damage and progression pattern of glaucoma in the peripapillary area (RNFL)[3,20,26,27] or macular area (GCIPL)[24] separately, and the result of the present study is similar to the results of these studies. However, our study differs in that it shows the spatial relations by combining the two areas and shows the changes in the initial progression-detected point and the last visit. This study is the first we know of to show the average progression pattern in the overall wide-field area using the newly proposed GPA PanoMap.

Our study has several limitations. First, as discussed elsewhere in this article, we did not analyze individual structural progressions. Because glaucoma progression can occur in various patterns, defining it as a uniform pattern can be a limitation. Second, stretching and rotating the images based on two landmark points may be unreasonable. However, the conventional analysis method does not consider all individual variations (e.g., FDA, fovea-disc distance, vascular distribution, disc size), so this factor can be considered. Third, we only enrolled the patients who were confirmed with structural progression with conventional structural images. Enrolled patients may have included many fast progressors, which can be difficult to generalize to the overall glaucoma patient. The high prevalence of disc hemorrhages, which typically are in the region of the disc associated with the MVZ, could act as selection bias. Last, we did not perform the analysis based on the stage of the disease and excluded patients with myopia. To obtain useful information

for the actual clinical situation, future studies considering this perspective into account are needed.

In conclusion, the patterns of progressive glaucomatous structural changes in both the peripapillary and macular areas were confirmed on the GPA PanoMap. This study applied commercially available combined RNFL and GCIPL GPA progression maps in the evaluation of the spatial characteristics and patterns of structural progression. The analysis of progression patterns using GPA PanoMap facilitates an improved understanding of the spatial relationship between the peripapillary and macular areas in glaucoma.

Acknowledgments

References

1. Lee EJ, Kim TW, Weinreb RN, Park KH, Kim SH, Kim DM. Trend-based analysis of retinal nerve fiber layer thickness measured by optical coherence tomography in eyes with localized nerve fiber layer defects. *Invest Ophthalmol Vis Sci*. 2011;52:1138–1144.

2. Leung CK. Diagnosing glaucoma progression with optical coherence tomography. *Curr Opin Ophthalmol*. 2014;25:104–111.

3. Leung CK, Cheung CY, Weinreb RN, et al. Evaluation of retinal nerve fiber layer progression in glaucoma: a study on optical coherence tomography guided progression analysis. *Invest Ophthalmol Vis Sci*. 2010;51:217–222.

4. Wollstein G, Schuman JS, Price LL, et al. Optical coherence tomography longitudinal evaluation of retinal nerve fiber layer thickness in glaucoma. *Arch Ophthalmol*. 2005;123:464–470.

5. Jeoung JW, Choi YJ, Park KH, Kim DM. Macular ganglion cell imaging study: glaucoma diagnostic accuracy of spectral-domain optical coherence tomography. *Invest Ophthalmol Vis Sci*. 2013;54:4422–4429.

6. Mwanza JC, Durbin MK, Budenz DL, et al. Glaucoma diagnostic accuracy of ganglion cell-inner plexiform layer thickness: comparison with nerve fiber layer and optic nerve head. *Ophthalmology*. 2012;119:1151–1158.

7. Jeong JH, Choi YJ, Park KH, Kim DM, Jeoung JW. Macular ganglion cell imaging study: covariate effects on the spectral domain optical coherence tomography for glaucoma diagnosis. *PLoS One*. 2016;11:e0160448.

8. Lee SY, Jeoung JW, Park KH, Kim DM. Macular ganglion cell imaging study: interocular symmetry of ganglion cell-inner plexiform layer thickness in normal healthy eyes. *Am J Ophthalmol*. 2015;159:315–323, e312.

9. Kim KE, Park KH. Macular imaging by optical coherence tomography in the diagnosis and management of glaucoma. *Br J Ophthalmol*. 2017;102:718–724.

10. Hood DC, Raza AS, de Moraes CG, Liebmann JM, Ritch R. Glaucomatous damage of the macula. *Prog Retin Eye Res*. 2013;32:1–21.

11. Kim YK, Ha A, Na KI, Kim HJ, Jeoung JW, Park KH. Temporal relation between macular ganglion cell-inner plexiform layer loss and peripapillary retinal nerve fiber layer loss in glaucoma. *Ophthalmology*. 2017;124:1056–1064.

12. Kim YK, Jeoung JW, Park KH. Inferior macular damage in glaucoma: its relationship to retinal nerve fiber layer defect in macular vulnerability zone. *J Glaucoma*. 2017;26:126–132.

13. Hood DC. Improving our understanding, and detection, of glaucomatous damage: an approach based upon optical coherence tomography (OCT). *Prog Retin Eye Res*. 2017;57:46–75.

14. Marshall HN, Andrew NH, Hassall M, et al. Macular ganglion cell-inner plexiform layer loss precedes peripapillary retinal nerve fiber layer loss in glaucoma with lower intraocular pressure. *Ophthalmology*. 2019;126:1119–1130.

15. Lee WJ, Oh S, Kim YK, Jeoung JW, Park KH. Comparison of glaucoma-diagnostic ability between wide-field swept-source OCT retinal nerve fiber layer maps and spectral-domain OCT. *Eye (London, England)*. 2018;32:1483–1492.

16. Lee WJ, Na KI, Kim YK, Jeoung JW, Park KH. Diagnostic ability of wide-field retinal nerve fiber layer maps using swept-source optical coherence tomography for detection of preperimetric and early perimetric glaucoma. *J Glaucoma*. 2017;26:577–585.

17. Lee WJ, Na KI, Ha A, Kim YK, Jeoung JW, Park KH. Combined use of retinal nerve fiber layer and ganglion cell-inner plexiform layer event-based progression analysis. *Am J Ophthalmol*. 2018;196:65–71.

18. Lee WJ, Kim TJ, Kim YK, Jeoung JW, Park KH. Serial combined wide-field optical coherence tomography maps for detection of early glaucomatous structural progression. *JAMA Ophthalmol*. 2018;136:1121–1127.

19. Hou HW, Lin C, Leung CK. Integrating macular ganglion cell inner plexiform layer and parapapillary retinal nerve fiber layer measurements to detect glaucoma progression. *Ophthalmology*. 2018;125:822–831.

20. Leung CK, Yu M, Weinreb RN, Lai G, Xu G, Lam DS. Retinal nerve fiber layer imaging with spectral-domain optical coherence tomography: patterns of retinal nerve fiber layer progression. *Ophthalmology*. 2012;119:1858–1866.

21. Suh MH, Kim DM, Kim YK, Kim TW, Park KH. Patterns of progression of localized retinal nerve fibre layer defect on red-free fundus photographs in normal-tension glaucoma. *Eye (London, England)*. 2010;24:857–863.

22. Mills RP, Budenz DL, Lee PP, et al. Categorizing the stage of glaucoma from pre-diagnosis to end-stage disease. *Am J Ophthalmol*. 2006;141:24–30.

23. Lee WJ, Kim YK, Park KH, Jeoung JW. Trend-based analysis of ganglion cell-inner plexiform layer thickness changes on optical coherence tomography in glaucoma progression. *Ophthalmology*. 2017;124:1383–1391.

24. Shin JW, Sung KR, Lee GC, Durbin MK, Cheng D. Ganglion cell-inner plexiform layer change detected by optical coherence tomography indicates progression in advanced glaucoma. *Ophthalmology*. 2017;124:1466–1474.

25. Hood DC, Nguyen M, Ehrlich AC, et al. A test of a model of glaucomatous damage of the macula with high-density perimetry: implications for the locations of visual field test points. *Transl Vis Sci Technol*. 2014;3:5.

26. Lin C, Mak H, Yu M, Leung CK. Trend-based progression analysis for examination of the topography of rates of retinal nerve fiber layer thinning in glaucoma. *JAMA Ophthalmol*. 2017;135:189–195.

27. Xu G, Weinreb RN, Leung CKS. Retinal nerve fiber layer progression in glaucoma: a comparison between retinal nerve fiber layer thickness and retardance. *Ophthalmology.* 2013;120:2493–2500.

28. Hood DC, Raza AS. On improving the use of OCT imaging for detecting glaucomatous damage. *Br J Ophthalmol.* 2014;98(Suppl. 2):ii1–ii9.

29. Mwanza JC, Lee G, Budenz DL. Effect of adjusting retinal nerve fiber layer profile to fovea-disc angle axis on the thickness and glaucoma diagnostic performance. *Am J Ophthalmol.* 2016;161:12–21, e11-e12.

30. Hong SW, Ahn MD, Kang SH, Im SK. Analysis of peripapillary retinal nerve fiber distribution in normal young adults. *Invest Ophthalmol Vis Sci.* 2010;51:3515–3523.